Analysis of E × B drifts in Earths magnetosphere during geomagnetic reversals: potential consequences for plasmasphere behavior and stability

J. A. Caggiano[1]and C. S. Paty[1]

[1]Department of Earth Sciences, University of Oregon, Eugene, OR 97403.

Key Points:

- Pole reversals dramatically affect electric fields and plasmasphere stability due to changes in the topology of Earths magnetic field.
- Quadrupole magnetic field topologies generate sunward convection flows in one hemisphere, and tailward convection flows in the other hemisphere. Quadrupole topologies that exhibit rotational modulation with respect to the solar wind do not support steady-state convection and result in stronger plasmasphere erosion.
- The plasmapause and magnetopause boundary positions are sensitive to changes in magnetic field strength and are highly dependent on magnetic field topology.

Corresponding author: J. A. Caggiano, jcaggian@uoregon.edu

Abstract

Geomagnetic pole reversals occur frequently throughout geologic history, although one has not yet occurred in recorded time. Magnetohydrodynamic models of Earths core have revealed that during a reversal, the magnetic dipole moment disappears, leaving higher-order moments. Previous research examined quadrupole magnetic field topologies and quantitatively specified the magnetic equators of those topologies but did not fully examine charged particle drift motion and stability in the inner magnetosphere. Earths closed magnetosphere is primarily dominated by two electric fields, the corotational and convection generated electric fields. $\vec{E} \times \vec{B}$ drifts from these fields ultimately drives the behavior of the cold plasma of the plasmasphere. In a quadrupole-dominated magnetic field, the plasma motion generated by the $\vec{E} \times \vec{B}$ drifts would be dramatically different from the classical dipole field plasma convection. Three quadrupole topologies were evaluated, and the $\vec{E} \times \vec{B}$ drift was analyzed along the magnetic equators of these topologies to characterize and quantify the resultant plasma motion and evaluate the behavior, structure and stability of the plasmasphere. We also tested for plasmaspause and magnetopause boundary sensitivity to magnetic field strength. The direction of the convection flow is hemispherically dependent for the $\eta = 0$ and 0.5 quadrupole topologies, that is, the plasma in the Northern Hemisphere convects tailward, and the Southern Hemisphere convects sunward. The $\eta = 1$ topology demonstrates evidence of strong plasmasphere erosion due to the intersection of the magnetic equators, and is particularly sensitive to reductions in magnetic field strength.

Plain Language Summary

Earth's magnetic field protects the planet from high-energy particles from the Sun. Little is known about what happens to Earths magnetic field during a geomagnetic pole reversal, yet pole reversals occur regularly on geological timescales. Previous studies suggested that during pole reversals, Earth's magnetic field becomes more complex, taking on the appearance of magnetic quadrupoles, and the overall magnetic field strength decreases. We studied the effects a pole reversal would have on Earth's electric fields, and how that would affect the cold, atmosphere-sourced plasma in the near-Earth space environment known as the plasmasphere. We find that the stability of the plasmasphere is highly dependent on the shape of the magnetic field, and that magnetic field shapes lacking a symmetry around Earth's rotational axis lead to stronger erosion of Earth's plasmasphere, and leaves Earth's atmosphere more vulnerable to changes in magnetic field strength.

1 Introduction

Geomagnetic pole reversals occur consistently on Earth through geologic time scales, the latest reversal occurring approximately 781,000 years ago (Lowrie & Kent, 1983; Singer & Coe, 2019). Pole reversals, and even geomagnetic excursions, are though to have profound effects on Earth's climate, biosphere and other surface processes (Cooper et al., 2021). However, little is known about the topology of Earth's magnetic field during a pole reversal process. Magnetohydrodynamic (MHD) geodynamo modelling of the Earths core by Glatzmaier and Roberts (1995) has shown that during the relatively brief time period of a pole reversal the dipole moment of the magnetic field tends to disappear in favor of higher-order magnetic moments. Of the higher-order magnetic moments, the quadrupole moment decays the least with respect to distance from Earth and is therefore thought to dominate the magnetic field (Vogt & Glassmeier, 2000).

Understanding the influence of quadrupole magnetic moments on magnetospheric dynamics in general will help provide insight into Earth's magnetosphere during a pole reversal, as well as the present-day magnetospheres of other planets within the Solar System. While a pure quadrupole magnetic field has not yet been observed in a planetary body, many of the planets in our Solar System, such as Mercury, Uranus and Neptune, possess signifi-

cant quadrupole moments (Takahashi & Tsunakawa, 2019; Connerney & Ness, 1987; Ness & Neubauer, 1989). For simplicity and convenience, the magnetic fields of said planetary bodies are typically represented as dipole moments that are offset from the planet's center and tilted with respect to the planetary rotation axis. However, in terms of alluding to generation mechanisms the fields are more accurately described as a combination of dipole and quadrupole moments. Describing the importance and influence of strong quadrupole moments is critical for a realistic understanding of planetary magnetospheric dynamics, especially in the inner magnetosphere where the higher order magnetic moments are strongest.

Vogt and Glassmeier (2000) derived magnetic field equations and magnetic equators for three symmetric quadrupole topologies (Figure 1) and demonstrated that magnetospheric plasma dynamics could behave quite differently during a pole reversal than during a normal dipole-dominated magnetosphere. However, the scope of Vogt and Glassmeier (2000) only extended to mapping of magnetic equipotential lines on the magnetic equators of these quadrupole fields in order to explore the bounce motion of plasma particles in the near-Earth environment. Their study did not consider the effects of electric fields on drifting plasma.

The nature of magnetospheric convection has a significant effect on the motion of low-energy plasma in the inner magnetosphere (Kavanaugh et al., 1968). This effect is mainly driven by $\vec{E} \times \vec{B}$ drifts associated with the planetary magnetic field and the local electric fields. The main electric fields are the corotational electric field caused by the rotation of Earth's intrinsic magnetic field and the convection electric field is generated from the magnetospheric convection due to the interactions of Earth's magnetosphere with the solar wind (Nishida, 1966). Volland (1973) and Stern (1974) semi-empirically derived an analytical model for the convection electric field for a dipole field by calculating the -$\vec{v} \times \vec{B}$ electric potential generated by the solar wind across the poles, and extending the potential across the magnetic equator where closed-field convection occurs in a dipole dominated magnetosphere.

Vogt et al. (2004) studied tail currents in the same quadrupole magnetic fields using the BATS-R-US single-fluid MHD model. The results from their ideal MHD model were quite remarkable in the sense that the model produced a convection profile of Earths magnetosphere that is dramatically different from the dipole magnetospheric convection that we see today. However, the unconventional nature of magnetospheric convection in the quadrupole field was largely unaddressed by the Vogt et al. (2004) study.

In this study, we assess the Volland-Stern magnetospheric potential model validity for a quadrupole magnetosphere. We also examine the affect of the quadrupole field on magnetospheric convection and analyze the corotational and convection electric fields and their associated $\vec{E} \times \vec{B}$ drift trajectories for several quadrupole magnetic field topologies and use the results to infer the stability of Earths plasmasphere in the event of a pole reversal.

2 Methods

2.1 Magnetic Quadrupole Topologies

The quadrupole magnetic field topologies are derived using spherical harmonics. Following the derivation from Vogt and Glassmeier (2000), the scalar potential of a magnetic quadrupole is expressed as:

$$\Psi = \frac{1}{2} \sum_{i,j=1}^{3} Q_{ij} \frac{x_i x_j}{\vec{r^5}} \tag{1}$$

Where $\vec{r}$ is the radius from the center of the Earth and Q_{ij} is the quadrupole tensor, defined as:

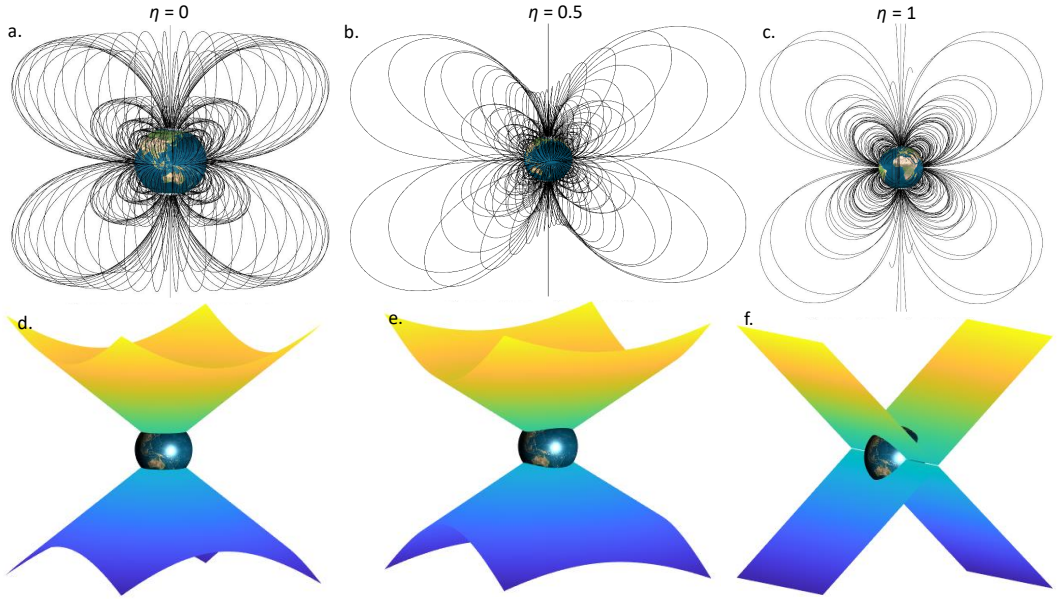

Figure 1. Magnetic quadrupole topologies used in the study. (a) Quadrupole field using the $\eta = 0$ shape parameter, (b) using the $\eta = 0.5$ shape parameter and (c) using the $\eta = 1$ shape parameter. (d-f) Magnetic equatorial surfaces for each quadrupole topology, respectively. For the purposes of illustration, the magnetic equatorial surfaces are rotated 25 degrees to show asymmetries.

$$Q_{ij} = q \cdot \begin{pmatrix} -\frac{1-\eta}{2} & 0 & 0 \\ 0 & -\frac{1+\eta}{2} & 0 \\ 0 & 0 & 1 \end{pmatrix} \tag{2}$$

In (2), q is a scaling parameter, which for this study is set equal to 1. The shape parameter term, η, is what drives the differences in topologies. The η parameter, defined in detail by Vogt and Glassmeier (2000), is a ratio of Schmidt coefficients from the spherical harmonic expansion of the quadrupole scalar potential such that:

$$\eta = \frac{\sqrt{3} g_2^2}{g_2^0} \tag{3}$$

For the purposes of this study, we used the values 0, 0.5 and 1 for η to explore a wide range of quadrupole topologies. Negative values of η are not explored because they present the same geometry as positive values but with reversed magnetic moments. The magnetic field equations are determined for each shape parameter by taking the negative gradient of (1):

$$\vec{B} = -\nabla \Psi \tag{4}$$

Equation (4) delineates the magnetic fields for the shape parameters specified above. These magnetic fields are visualized in Figure 1. Our magnetic fields are defined so the magnetic field axis is aligned with Earth's rotational axis. This alignment is is performed as a simplifying assumption that is reasonable for Earth, and allows for direct comparison to the The Volland (1973) and Stern (1974) convection potential derivations, which make the same assumption.

The magnetic equator is defined as a surface or set of surfaces where the magnetic field gradient reaches a local minimum. This is quantitatively defined as:

$$\vec{B}^T(\nabla\vec{B})\vec{B} = 0 \tag{5}$$

The equatorial surfaces produced are shown in Figure 1d-f.

2.2 Electric Fields and E × B Drifts

As the Earth rotates, the magnetic field rotates with it. This generates a -$\vec{v} \times \vec{B}$ corotational electric field around earth. The corotational electric field is defined as:

$$\vec{E}_{CR} = \vec{\Omega} \times \vec{r} \times \vec{B} \tag{6}$$

where $\vec{\Omega}$ is the angular velocity vector of the Earth in the direction of the rotation axis, $\vec{r}$ is the position vector from the center of the Earth, and $\vec{B}$ is the magnetic field (Maus, 2017).

The convection electric field is a -$\vec{v} \times \vec{B}$ electric field brought on by the sunward flow of Earths magnetic field due to magnetospheric convection (Kavanaugh et al., 1968). This field exists within the closed magnetic field of Earths magnetosphere, although it is often projected on the equatorial plane of Earth since this is where the electric field is strongest due to the maximum convection velocity on this plane (Maus, 2017). The convection field is altered by the differential motion of ions and electrons around the Earth as plasma flows sunward via a shielding process. This shielding process is dependent on the plasma flux convecting around Earth, which is ultimately dependent on solar wind activity. The convection electric field accounting for shielding is defined via the Volland-Stern magnetospheric potential (Volland, 1973; Stern, 1974; Maynard & Chen, 1975), and is semi-empirically derived based on the electric field generated by the interplanetary magnetic field moving across Earth's polar caps. This electric field is projected onto the magnetic equator, and its electric potential can be written as:

$$\Phi_{CS} = \frac{92.4}{R} - AR^N \sin\phi \tag{7}$$

Where R is the radial distance from Earth's center, N is a parameter that is optimally equal to 2 based on work from Stern (1974), and ϕ is the angle from the subsolar point in the direction of Earth's rotation. A is the constant shielding factor based on the solar wind k_p-index, given by:

$$A = \frac{0.045}{(1 - 0.159k_p + 0.0093k_p^2)^3} \tag{8}$$

This study will assume a solar wind with a k_p-index value of 4 for the purposes of direct comparison to the Volland (1973) and Stern (1974) derivations. The convection electric field is the gradient of the Volland-Stern magnetospheric potential:

$$\vec{E}_{CS} = -\nabla\Phi_{CS} \tag{9}$$

These electric field equations are derived with the simplifying assumption that the magnetic equator for the dipole is located at the geographic equator. to simplify modelling efforts, the coordinate system is converted to Cartesian and defined such that $\hat{x}$ is tailward (away from the Sun), $\hat{y}$ is toward the dawn side of Earths magnetopause along the geographical equator, and $\hat{z}$ completes the right-hand coordinate system.

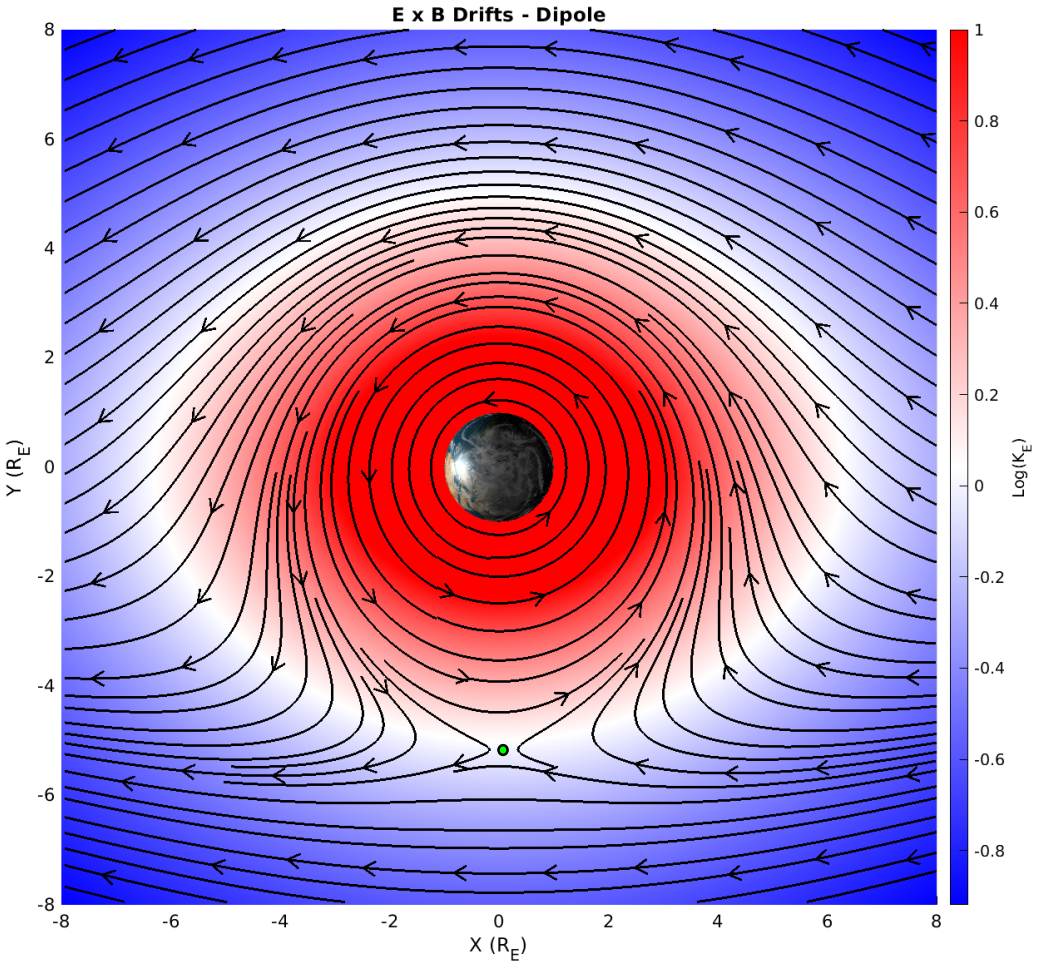

Figure 2. The $\vec{E} \times \vec{B}$ drift field streamlines around Earth on the magnetic/geographic equator. All space that is red is dominated by the Corotational E-Field, and all space in blue is Convection E-Field dominated. The green dot is the location of the stagnation point.

Both corotational and convection electric fields are important when describing the plasmasphere of Earth. The drift velocity of relatively cold plasma in the near-Earth environment is generated from several processes, of which the dominant mechanism is the $\vec{E} \times \vec{B}$ drift. The $\vec{E} \times \vec{B}$ drift velocity is quantitatively defined as:

$$\vec{v}_D = \frac{\vec{E} \times \vec{B}}{|\vec{B}|^2} \tag{10}$$

The plasma motion is primarily driven by the locally dominant electric field (Baumjohann & Treumann, 2012). Figure 2 demonstrates the influence of these electric fields on the $\vec{E} \times \vec{B}$ drift for charged particles in a dipole magnetic field. The color bar in Figure 2 (and following figures) denotes the regionally dominant electric field using a ratio, K_E of the relative strength of the corotational and convection electric fields across the magnetic equator surfaces was calculated.

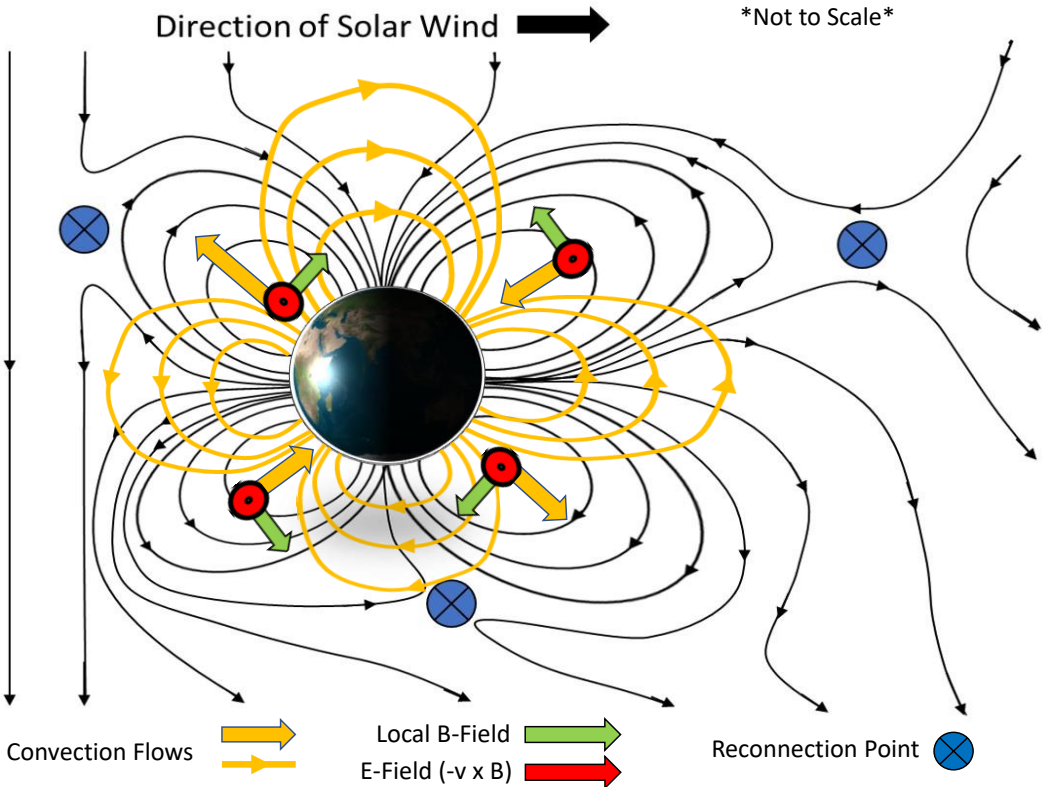

Figure 3. Conceptual illustration of the convection profile, flows, and calculated electric fields for a $\eta = 0$ quadrupole magnetic field.

$$K_E = \frac{|\vec{E}_{CR}|}{|\vec{E}_C|} \tag{11}$$

The plasmapause boundary is considered to be the location on the magnetic equatorial surface where the ratio of convection and corotational electric field magnitudes is unity. In regions where the dominant electric field is corotational (red), the plasma will continue drifting around the Earth. Whereas if the plasma encounters a convection-dominated electric field (blue), it will be eroded from the plasmasphere and drift sunward towards the magnetopause. The white region indicates where the magnitudes of the convective and corotational electric fields are balanced. There is a specific point on the dusk side of Earth where the $\vec{E} \times \vec{B}$ drifts of the corotation and convection electric fields are equal in magnitude and opposing, known as the stagnation point (Nishida, 1966; Brice, 1967; Kavanaugh et al., 1968; Baumjohann & Treumann, 2012). The stagnation points are indicated by green dots in all figures.

For the dipole magnetic field these electric fields are the most significant on the magnetic equator, which is near the geographic equator. However, in a quadrupole-dominated magnetosphere the magnetic equators are not located anywhere near the geographic equator (Vogt & Glassmeier, 2000). The magnetic equators also have curvature and complex geometries for certain quadrupole configurations (Vogt & Glassmeier, 2000) (Figure 2). The applicability of the Volland-Stern convection model must therefore be tested for a quadrupole.

2.3 Volland-Stern Magnetospheric Potential in a Quadrupole

Given the dipole-dependence of the Volland-Stern Magnetospheric Potential derivation, the question arises whether this convection model is useful for a quadrupole magnetosphere. This concern is addressed by examining the nature of the convection flows in a quadrupole magnetosphere. Figure 3 illustrates a conceptual map in the X-Z plane of a magnetic quadrupole field convecting while interacting with the solar wind with a southward interplanetary magnetic field. The convection and reconnection points in Figure 4 demonstrate that the quadrupole field can be divided into two hemispheric convection regions. One region shows magnetic reconnection occuring at the sunward magnetopause and in the magnetotail, which indicates open style convection. The other hemisphere reconnects with the solar wind tailward of the magnetospheric cusp, indicating a closed style convection region. Qualitative evaluation of the local -$\vec{v} \times \vec{B}$ electric fields for the quadrupole $\eta = 0$ reveals that the electric field and resultant $\vec{E} \times \vec{B}$ drift velocities are in the same direction that the Volland-Stern model predicts when applied to a quadrupole at all points in the evaluated space. A derivation of the general solution of the convection electric field is available in the Appendix.

2.4 Variable Field Strength

Several studies have suggested that the maximum surface field strength will decrease by approximately one order of magnitude (Glassmeier & Buchert, 2004; Siscoe & Sibek, 1980; Ultre-Geurard & Achache, 1995; Vogt et al., 2004). However, given the lack of observational constraint on changes to overall magnetic field strength during a pole reversal, we explored the sensitivity of the dipole and quadrupole plasmaspheres to changes in magnetic field strength to understand how the plasmasphere erodes with smaller magnetic field strengths. To do this, the surface magnetic field strength was evaluated at 0.05, 0.1, 0.2, 0.5, 1, 2, 5, and 10 times the present-day surface magnetic field strength of 31200 nT (Baumjohann & Treumann, 2012). The plasmapause location was then found along the magnetic equators of the Earth for each magnetic configuration and surface strength.

3 Results

Each magnetic quadrupole topology was tested by plotting streamlines tracing the $\vec{E} \times \vec{B}$ drift patterns along the magnetic equatorial surfaces, which are shaded based on the dominant electric field along the equatorial surfaces.

Figure 4 (Top) illustrates the $\vec{E} \times \vec{B}$ and electric field visualization for the quadrupole field calculated with the $\eta = 0$ shape parameter. The figure shows that Earth has two separate magnetic equator surfaces, and the $\vec{E} \times \vec{B}$ drift patterns in convection dominated regions are structured similarly. However, because the magnetospheric convection flows are opposite along the equatorial surfaces in each hemisphere, the $\vec{E} \times \vec{B}$ drifts for each hemisphere in the convection electric field region are travelling in opposite directions relative to each other. The plasma drift in the corotationally-dominated electric field regions continue to drift in the corotational direction. However, since each hemisphere of the plasmasphere encounters convection in opposite directions at the magnetic equators, two stagnation points appear on opposite sides of Earth on each magnetic equatorial surface.

A similar structure of opposing convection flows in each hemisphere regions is apparent for the $\eta = 0.5$ configuration (Figure 4 Bottom). The convection fields are also typical compared to the $\eta = 0$ topology. The corotational fields in this scenario are stable, albeit elongated due to the nature of the magnetic field topology. Due to the time dependent nature of a non-axisymmetric quadrupole, the elongated field rotates with the Earth. This implies that the stagnation points will oscillate radially and latitudinally relative to Earth. However, the closed nature of the corotational streamlines indicates that no enhancement of plasmasphere erosion is created from the oscillation.

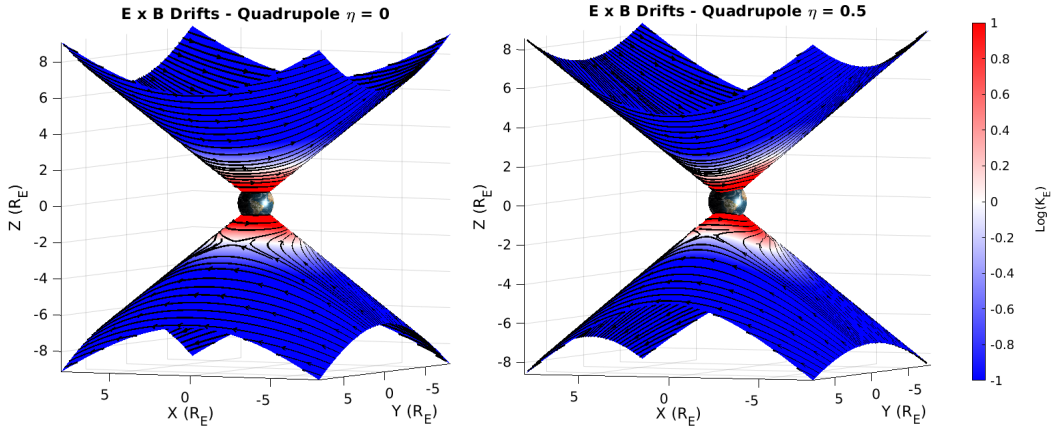

Figure 4. $\vec{E} \times \vec{B}$ streamlines along the magnetic equators for $\eta = 0$ (Left) and $\eta = 0.5$ (Right). The colors denote whether the region is in a corotational or convection dominated electric field . Note the reversal of convection flows on each equatorial surface.

The $\eta = 1$ topology (Figure 4) yields the most striking departure from canonical drift motion. For certain points in the rotation of Earth where the axis of equatorial surface convergence is oriented parallel/anti-parallel to the solar wind direction(Figure 4 - Top) the stagnation points are configured similarly to the $\eta = 0$ and 0.5 topologies in that each stagnation point is present on opposite sides of the planet for each hemisphere. The hemispheric regions also convect in opposite directions similarly to the other topologies. The main feature of interest, however, is the behavior of the drifts at the convergence zone of the two magnetic equators. The corotational electric field becomes significantly weaker with proximity to the magnetic equatorial surface convergence, causing the area to be mainly convection-dominated. Figure 5 shows a top-down view of the $\eta = 1$ drift configuration. This figure shows that when the corotationally-dominated plasma approaches the magnetic equator convergence zone, most of the plasma enters a convection electric field dominated area and is eroded away. This implies that a large portion of the plasmasphere would not survive a single drift period before being eroded away and is therefore unstable except at very low altitudes.

Because the $\eta = 1$ topology also rotates with Earth, the orientation of the field relative to the convection field is time dependent. This implies that the the axis of equatorial surface convergence will be periodically parallel and perpendicular to the magnetic convection flow. Figure 4 (Bottom) illustrates that when the the axis of equatorial surface convergence is perpendicular to the solar wind direction, the stagnation points disappear since no region exists where the corotational and convection $\vec{E} \times \vec{B}$ drifts directly oppose each other. The time dependent nature of $\eta = 1$ also causes the convection field to completely change directions in a time dependent matter, which is analyzed further in the discussion.

4 Discussion and Conclusions

The topology changes in the $\vec{E} \times \vec{B}$ fields indicate a significant change in the structure of the plasmasphere from the current dipole case. The streamlines mapped in Figure 4 indicate that the plasmasphere tracks along the magnetic equatorial surfaces, but each hemisphere is governed by opposing convection flows in the $\eta = 0$ and $\eta = 0.5$ cases. This was not the case for the $\eta = 1$ quadrupole, where the intersecting magnetic equators caused a significant reduction in the corotational electric field strength. This causes a large portion of the plasmasphere to erode into the convective field regime at this location. Therefore, the $\eta =$

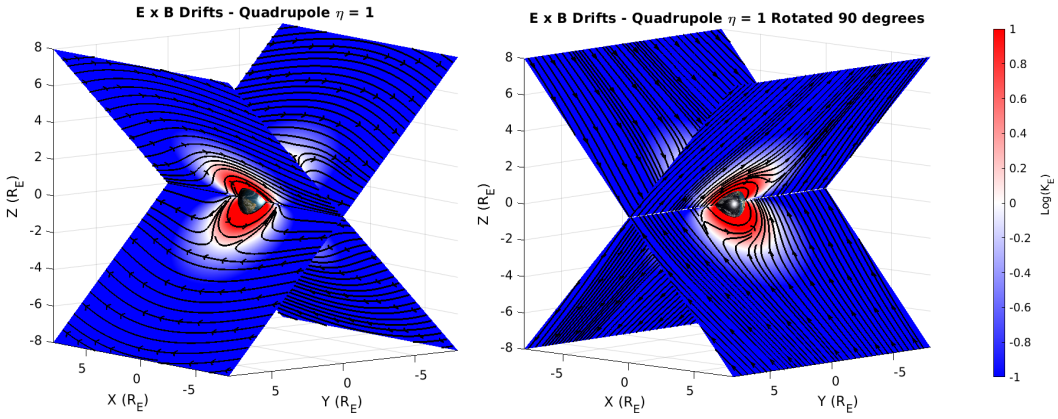

Figure 5. (Left) $\vec{E} \times \vec{B}$ streamlines along the magnetic equators for $\eta = 1$. The colors denote whether the region is on a corotation or convection field dominated region. (Right) $\vec{E} \times \vec{B}$ streamlines for the $\eta = 1$ magnetic field 6 hours later. Note the decrease of corotational domination where the equatorial surfaces converge.

1 geometry does not support a substantial plasmasphere because most of the material does not remain stable in the plasmasphere for more than one half of a drift orbit.

Development of a steady-state convection model for the quadrupole geometries is only feasible for the $\eta = 0$ case, due to the axisymmetry of the magnetic field. However, the non-axisymmetry and time dependent nature of the convection flows in $\eta = 0.5$ and 1 makes the quantitative derivation of a steady-state convection model impossible to calculate. The magnitude and orientation of magnetospheric convection changes periodically with rotation of the planet. While the $\eta = 0.5$

While this study presents a simplified, analytical solution to study plasmapause stability during a magnetic pole reversal, it does not account for dynamic effects such as magnetospheric compression, changes to the solar wind or plasmasphere erosion due to geomagnetic disturbances. To constrain the consequences of variable field strength of the magnetic topologies, the plasmapause locations were evaluated for a range of surface field strengths as described in Section 2.4. Figure 6 shows the minimum plasmapause radial distance as a function of surface magnetic field strength relative to the present-day value of 31200 nT. A standard dipole configuration produced the plasmasphere with the greatest radial extent and requires the magnitude of the surface magnetic field to be reduced by approximately two orders of magnitude for the plasmapause to become completely unstable and disappear. The quadrupole fields $\eta = 0$ and $\eta = 0.5$ demonstrated a significantly weaker plasmasphere than a dipole but were still robust in that they required a similar reduction in magnetic field strength as the dipole for the plasmasphere to disappear completely. The $\eta = 1$ quadrupole, produced by far the most anemic plasmasphere, with a very close plasmapause at the magnetic equator convergence zone. At the modern-day magnetic field strength, the plasmapause is less than 1 Earth radius away from the surface. The surface field strength would only need to decrease to 1/4 of the current magnetic field strength for the plasmasphere to become completely unstable and disappear.

For a more complete exploration of the magnetic field strength parameter space, the sunward magnetopause boundary was located for each of the magnetic topologies (Figure 6). The magnetopause calculation assumed an average solar wind of 10 protons/cm3 travelling at 450 km/s. To get the most conservative magnetopause boundary estimate, the dynamic pressure from the solar wind was aligned with the magnetic equators for each magnetic field topology. This eliminated any obliqueness to the force balance, and pushed the magne-

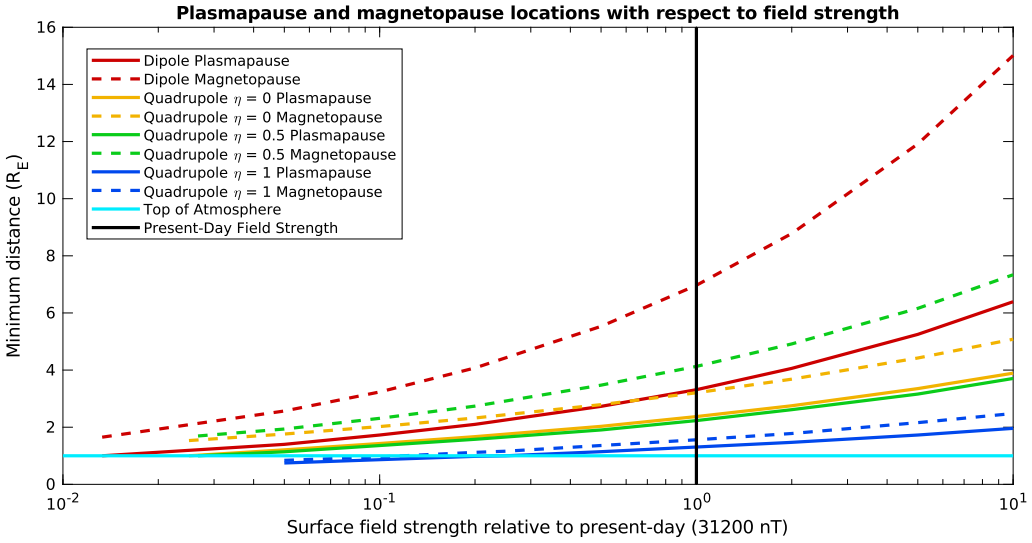

Figure 6. Plasmapause boundaries (Solid Lines) and the sunward magnetopause boundary (Dashed Lines) for each magnetic field topology at varying surface field strengths. The top of the atmosphere (Cyan Line at the Bottom) and the current field strength (Vertical Black Line) are also displayed.

topause boundary as close to Earth as possible. The calculated magnetopauses were found to be farther away from Earth than the plasmapause boundaries, which demonstrated that the plasmaspheres generated by the quadrupoles would be stable for magnetospheres compressed by standard solar wind conditions. For the $\eta = 1$ geometry when the field was less than 1/5 of its current strength the plasmapause and magnetopause boundaries are pushed below Earth's surface. If the magnetic field strength decreases by an order of magnitude as suggested in Section 2.4, and the magnetic field resembles an $\eta = 1$ configuration, the Earth and existing space-based assets will be directly exposed to the solar wind.

In summary, this study demonstrated the strong impact of quadrupole magnetic fields on the $\vec{E}\times\vec{B}$ drift and the structure and stability of the plasmasphere, highlighting the potential changes to Earth's near space environment during a magnetic reversal and highlighting potential differences in the dynamics of quadrupole-dominant planetary magnetospheres.

- Two of the quadrupole magnetic field topologies ($\eta = 0$, 0.5) create two plasmasphere regions around the corresponding magnetic equatorial surfaces. One is effected by a sunward magnetospheric convection, and the other by a tailward magnetospheric convection. There are also oppositely located stagnation points for each magnetic equator.
- The $\eta = 1$ quadrupole topology produces a weak plasmasphere that erodes significantly at the magnetic equator intersections. This causes the plasmasphere to become unstable since most of the plasma does not survive a single orbit around the planet.
- The axisymmetric $\eta = 0$ Quadrupole field is the only field topology that allows for derivation of a steady-state convection model. The other field topologies have time-dependent convection magnitudes and orientations, and thus can never achieve a steady state.
- The effect of changes to magnetic field strength on the plasmaphere and magnetosphere boundaries are strongly dependent on magnetic field topology.

The analytical solutions and sensitivity analysis presented in this paper provide insight into to understanding the stability of the plasmasphere during magnetic reversals. We found that the structure of the plasmasphere and sensitivity of the plasmasphere to changes in the magnetic field strength are very dependent on the topology of the magnetic field present during the reversal process. These characteristics deviate dramatically from the canonical present-day dipole plasmasphere. However, we do not examine the dynamic response of the magnetosphere to variability in the solar wind, and leave the implementation of a 3-dimensional plasma dynamic simulation to fully characterize the Earth's near-space environment to a future paper.

5 Appendix: Derivation of Volland-Stern Convection Potential

Volland (1973) and Stern (1974) semi-empirically derived the Convection electric potential using Euler potentials, which are scalar functions that characterize a plane perpendicular to the magnetic field at any given point in space such that:

$$\nabla\alpha \times \nabla\beta = \vec{B} \tag{12}$$

Where α and β are the Euler potentials of the magnetic field which represent two scalar functions that are orthogonal to each other and capable of describing the , and $\vec{B}$ is the magnetic field. Given the innate perpendicularity of the Euler potentials, they also satisfy the following conditions:

$$\nabla\alpha \cdot \vec{B} = 0 \tag{13}$$

$$\nabla\beta \cdot \vec{B} = 0 \tag{14}$$

The above equations are quasi-linear partial differential equations. This also implies that the Euler potentials are unique general solutions to the same quasilinear partial differential equations. For an axisymmetric magnetic field, the convection electric field and $\vec{E} \times \vec{B}$ drift field are assumed to be orthogonal to the magnetic field, and thus may also serve as representations of the gradients of the Euler potentials α and β as shown below.

$$\vec{E} \cdot \vec{B} = 0 \tag{15}$$

$$(\frac{\vec{E} \times \vec{B}}{B^2}) \cdot \vec{B} = 0 \tag{16}$$

This relationship indicates that α and β represent the scalar potentials of the convection electric field and the $\vec{E} \times \vec{B}$ drift fields. Our study departs from the Volland (1973) and Stern (1974) derivations by calculating the general solutions for the $\eta = 0$ quadrupole instead of a magnetic dipole. Solving the quasilinear partial differential equations for each Euler potential in the $\eta = 0$ topology produces the following general solutions:

$$\alpha = C_1 \frac{y}{x} \tag{17}$$

$$\beta = \ln \frac{(x^2 + y^2 + z^2)^{5/2}}{x^2 z} \tag{18}$$

The gradients of these general solutions reveal patterns very similar to the convection electric fields and $\vec{E} \times \vec{B}$ fields anticipated from previous research for the quadrupole field with shape parameter $\eta = 0$ (Figure A). The convection electric field vectors and $\vec{E} \times \vec{B}$ matches what is predicted from the illustration in figure 3.

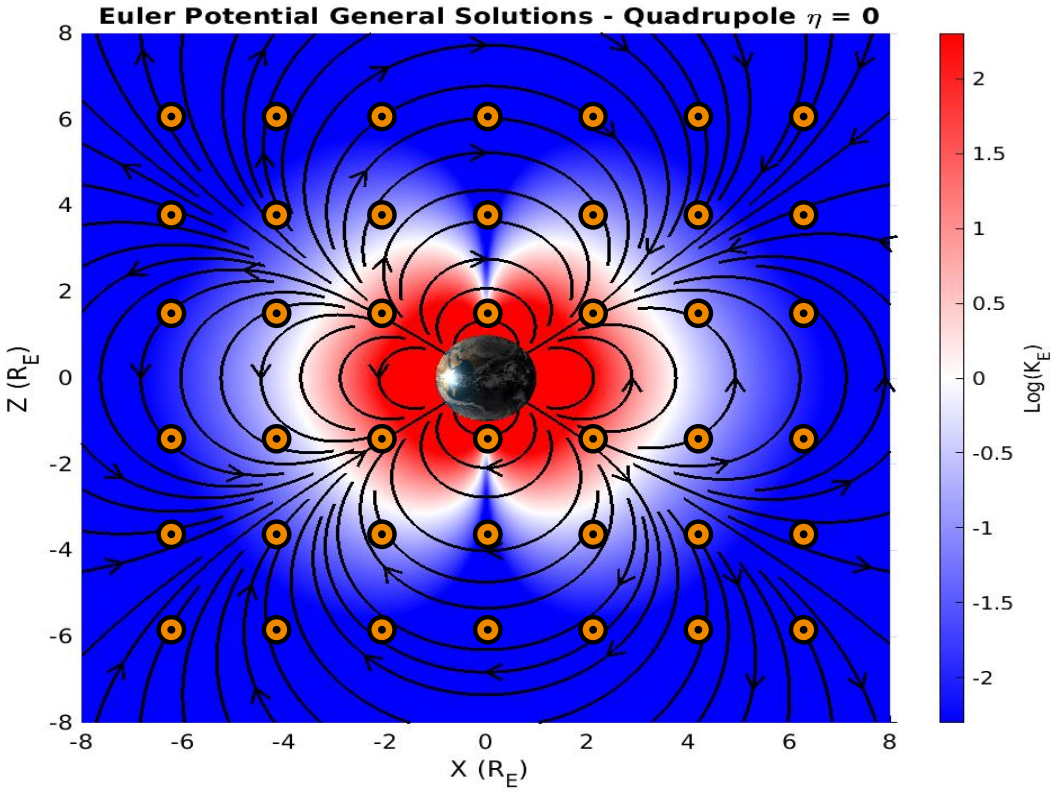

Figure A. General solutions for the Euler potentials. Black streamlines correspond to the $\vec{E} \times \vec{B}$ Euler potentials, and the orange vectors pointing out of the figure are the $\vec{E}$ Euler potentials. Colormap indicates the dominant electric field. Note the similarity of the $\vec{E} \times \vec{B}$ and $\vec{E}$ streamlines to those illustrated in Figure 3.

Solving for the particular solutions to the differential equations above, which correspond to the scalar potentials for the convection electric field and the $\vec{E} \times \vec{B}$ drift fields, requires knowledge of simplifying boundary conditions. The Volland (1973) and Stern (1974) derivations opted to rely on an empirical derivation based on observational data for their dipole case. However, no such luxury exists for the magnetic quadrupole case at this time. This makes the derivation of the particular solutions for the scalar potentials impossible without making bold simplifying assumptions. However, given how well the general solutions fit the hypothesized convection model as-is, the particular solutions would only serve to slightly refine the scalar potential structures.

Acknowledgments

Data sharing is not applicable to this article as no datasets were generated or analysed during the current study. The authors would like to thank the University of Oregon for funding this study via a First-Year Fellowship. There are no real or perceived conflicts of interests amongst the authors, financially or otherwise. The authors would also like to thank P. Regensburger, A. Olsen, A. Broz and M. Styczinski for their valuable commentary which led to the improvement of this paper.

References

Baumjohann, W., & Treumann, R. A. (2012). *Basic space plasma physics*. London: Imperial Coll. Press.

Brice, N. M. (1967). Bulk motion of the magnetosphere. *J. Geophys. Res.*, *72*, 5193-5211.

Connerney, M. H. A., J. E. P., & Ness, N. F. (1987). The magnetic field of uranus. *JGR Space Physics*, *92*, 15329-15336.

Cooper, A., et al. (2021). A global environmental crisis 42,000 years ago. *Science*, *371*, 811-818.

Glassmeier, J. V. A. S., K. H., & Buchert, S. (2004). Concerning long-term geomagnetic variations and space climatology. *Annales Geophysicae*, *22*, 3669-3677.

Glatzmaier, G. A., & Roberts, P. H. (1995). A three-dimensional self-consistent computer simulation of a geomagnetic field reversal. *Nature*, *377*, 203-209.

Kavanaugh, L. D. J., et al. (1968). Plasma flow in the magnetosphere. *J. Geophys. Res.*, *73*, 5511-5519.

Lowrie, W., & Kent, D. V. (1983). Geomagnetic reversal frequency since the late cretaceous. *Earth and Planetary Science Letters*, *62*, 305-313.

Maus, S. (2017). A corotation electric field model of the earth derived from swarm satellite magnetic field measurements. *JGR Space Physics*, *122*, 8733-8754.

Maynard, N. C., & Chen, A. J. (1975). Isolated cold plasma regions: observations and their relation to possible production mechanisms. *J. Geophys. Res.*, *80*, 1009-1013.

Ness, M. H. A. L. F. B. J. E. P. C. R. P. L., N. F., & Neubauer, N. F. (1989). Magnetic fields at neptune. *Science*, *246*, 1473-1478.

Nishida, A. (1966). Formation of plasmapause, or magnetospheric plasma knee, by the combined action of magnetospheric convection and plasma escape from the tail. *J. Geophys. Res.*, *71*, 5669-5679.

Singer, B. R. J. N. M., B. S., & Coe, R. S. (2019). Synchronizing volcanic, sedimentary, and ice core records of earths last magnetic polarity reversal. *Science Advances*, *5*, eaaw4621.

Siscoe, G. L., & Sibek, D. G. (1980). Effects of nondipole components on auroral zone configurations during weak dipole field epochs. *J. Geophys. Res.*, *85*, 3549-3556.

Stern, D. (1974). A model of the terrestrial electric field (abstract). *Eos Trans. AGU*, *55*, 403.

Takahashi, H. S., F., & Tsunakawa, H. (2019). Mercurys anomalous magnetic field caused by a symmetry-breaking self-regulating dynamo. *Dynamics, Structure and Evolution of the Earth and Planets*, *10*, 208.

Ultre-Geurard, P., & Achache, J. (1995). Core flow instabilities and geomagnetic storms during reversals: The steens mountain impulsive field variations revisited. *Earth and Planetary Science Letters*, *135*, 91-99.

Vogt, J., & Glassmeier, K. H. (2000). On the location of trapped particle populations in quadrupole magnetospheres. *J. Geophys. Res.*, *105*, 13063-13071.

Vogt, J., et al. (2004). Mhd simulations of quadrupole magnetospheres. *JGR Space Physics*, *109*, A12221.

Volland, H. (1973). A semiempirical model of large-scale magnetospheric electric fields. *J. Geophys. Res.*, *78*, 171.

Figure 1.

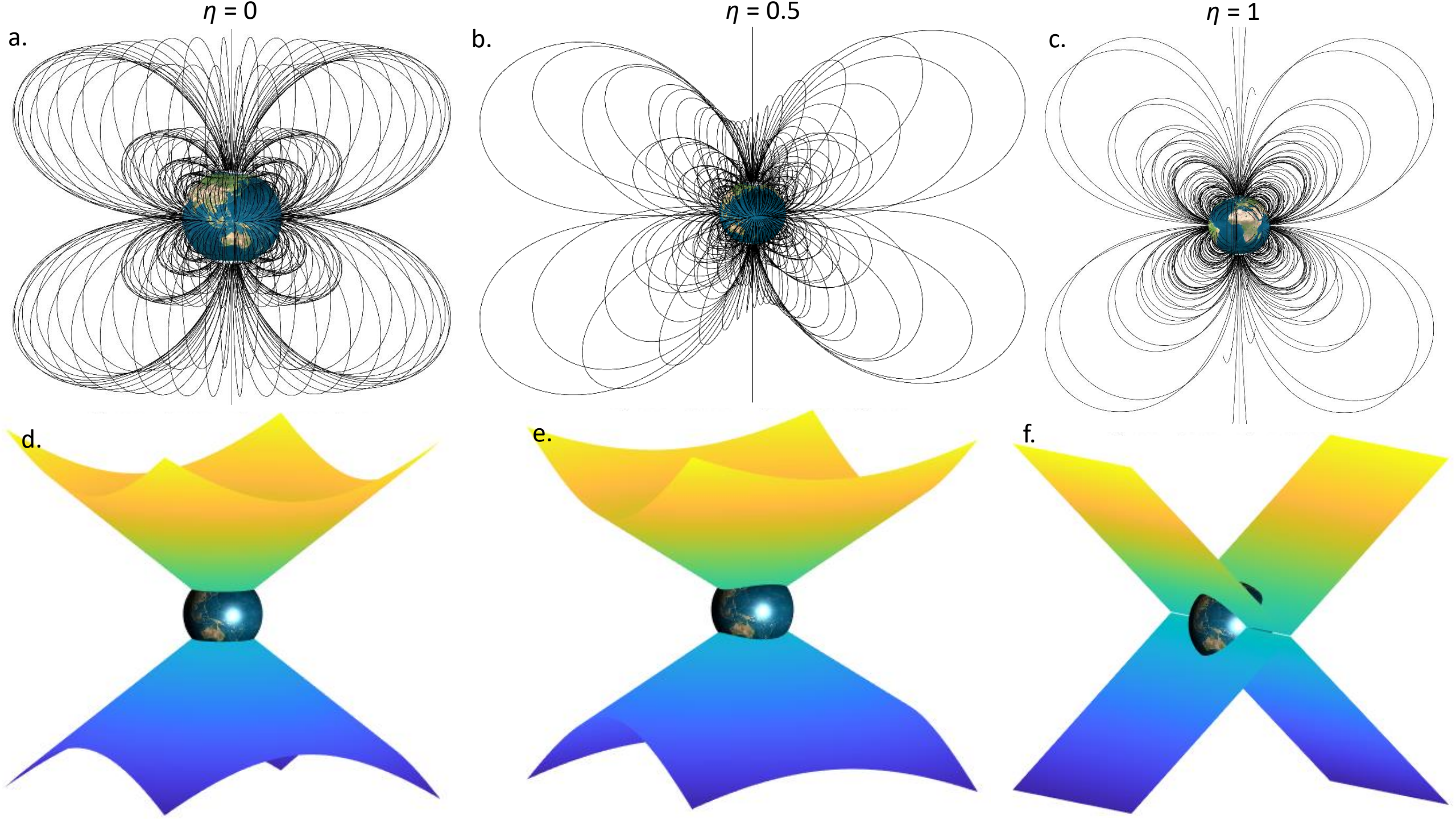
η = 0
η = 0.5
η = 1
a.
b.
c.
d.
e.
f.

Figure 2.

E x B Drifts - Dipole

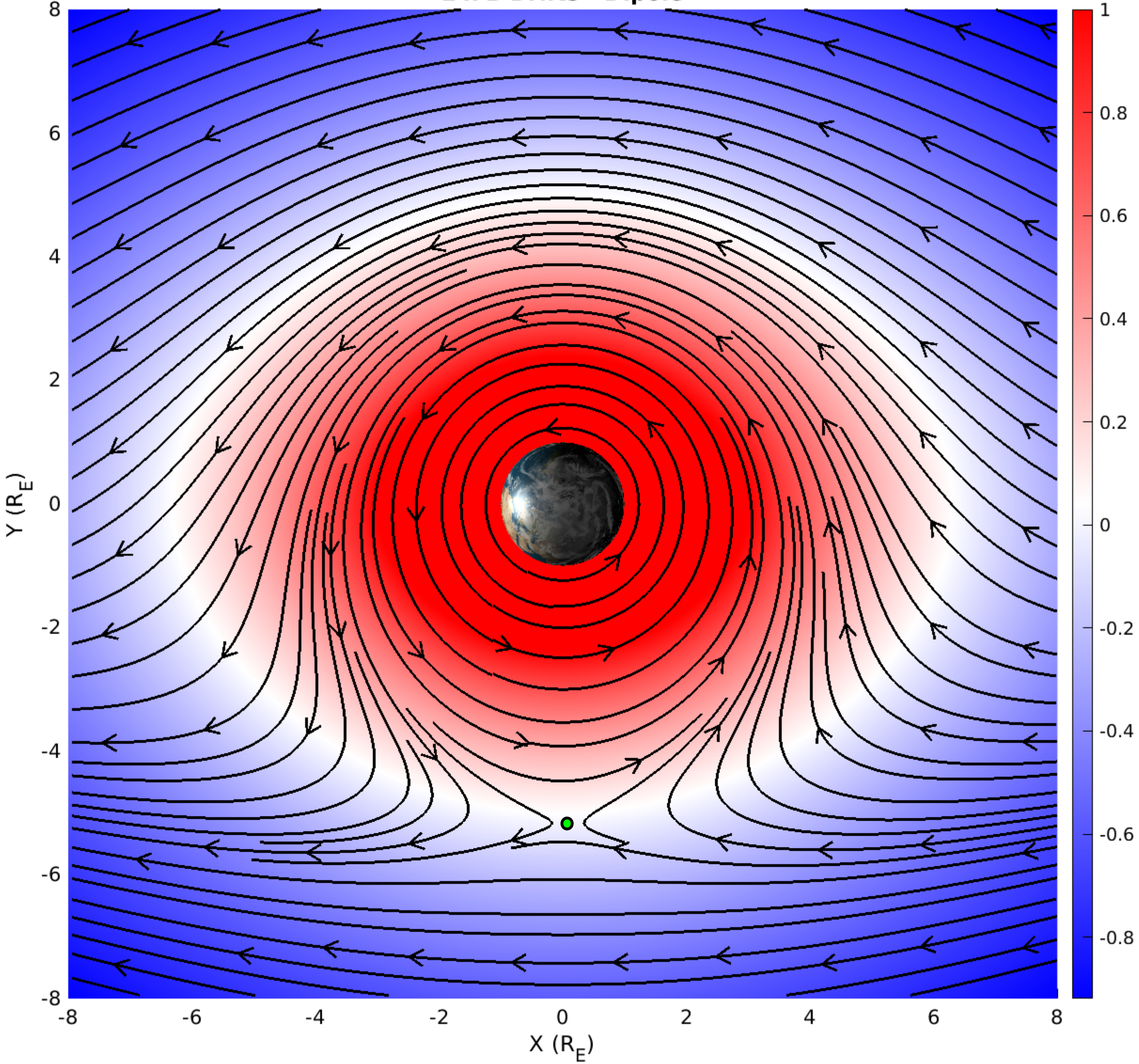

Figure 3.

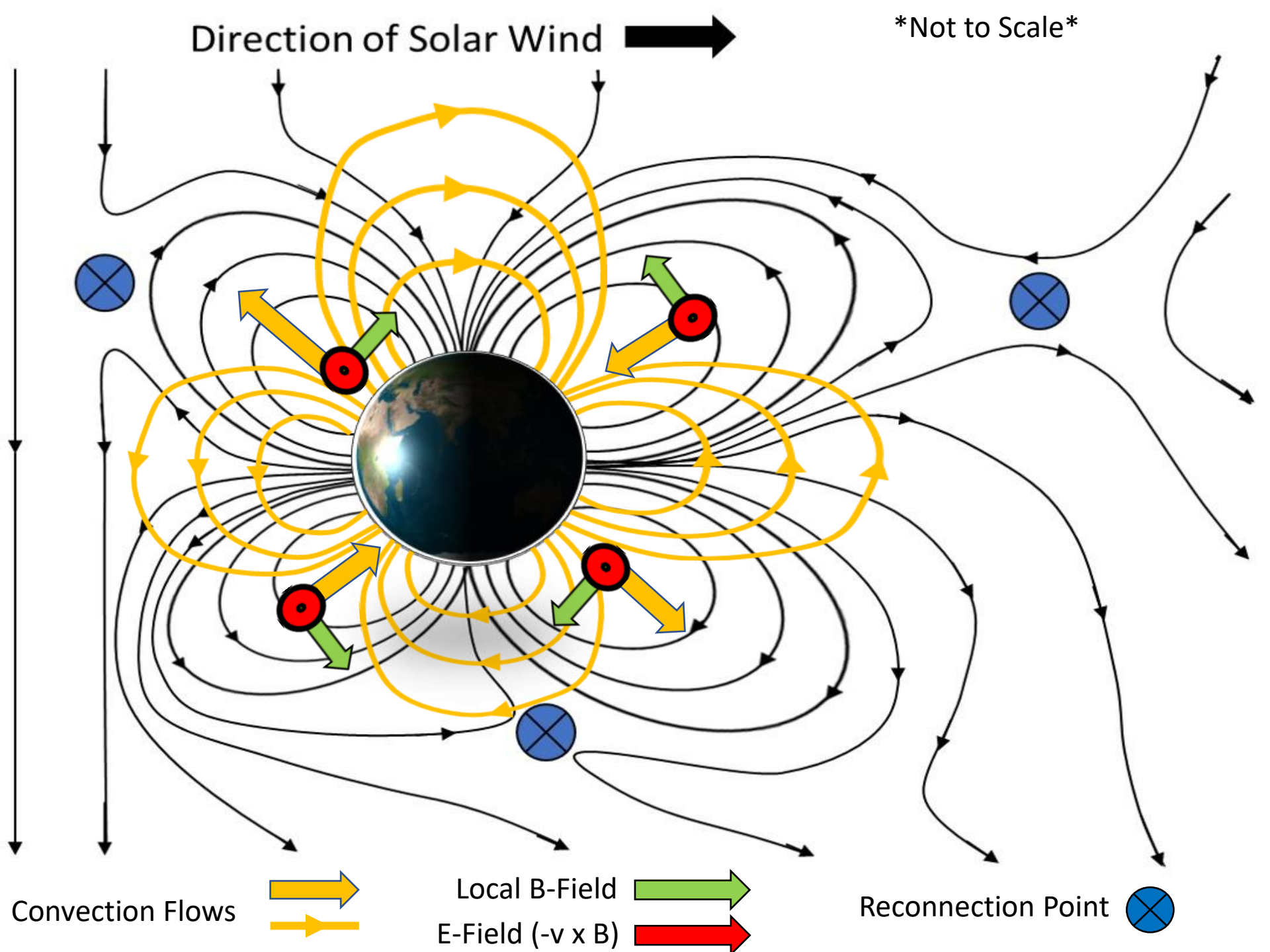
Direction of Solar Wind
Not to Scale
Convection Flows
Local B-Field
E-Field (-v x B)
Reconnection Point

Figure 4.

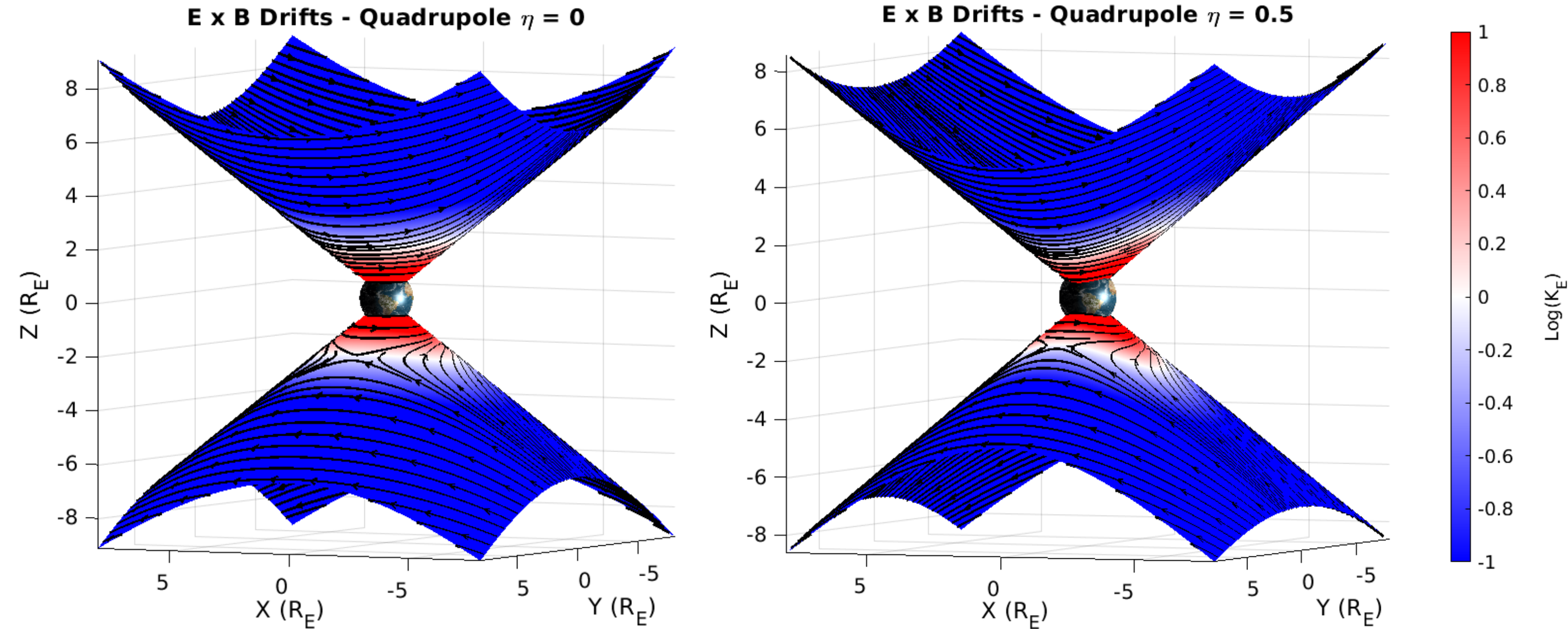
E x B Drifts - Quadrupole η = 0
E x B Drifts - Quadrupole η = 0.5
Z (R_E)
X (R_E)
Y (R_E)
Log(K_E)
8
6
4
2
0
-2
-4
-6
-8
5
0
-5
1
0.8
0.6
0.4
0.2
0
-0.2
-0.4
-0.6
-0.8
-1

Figure 5.

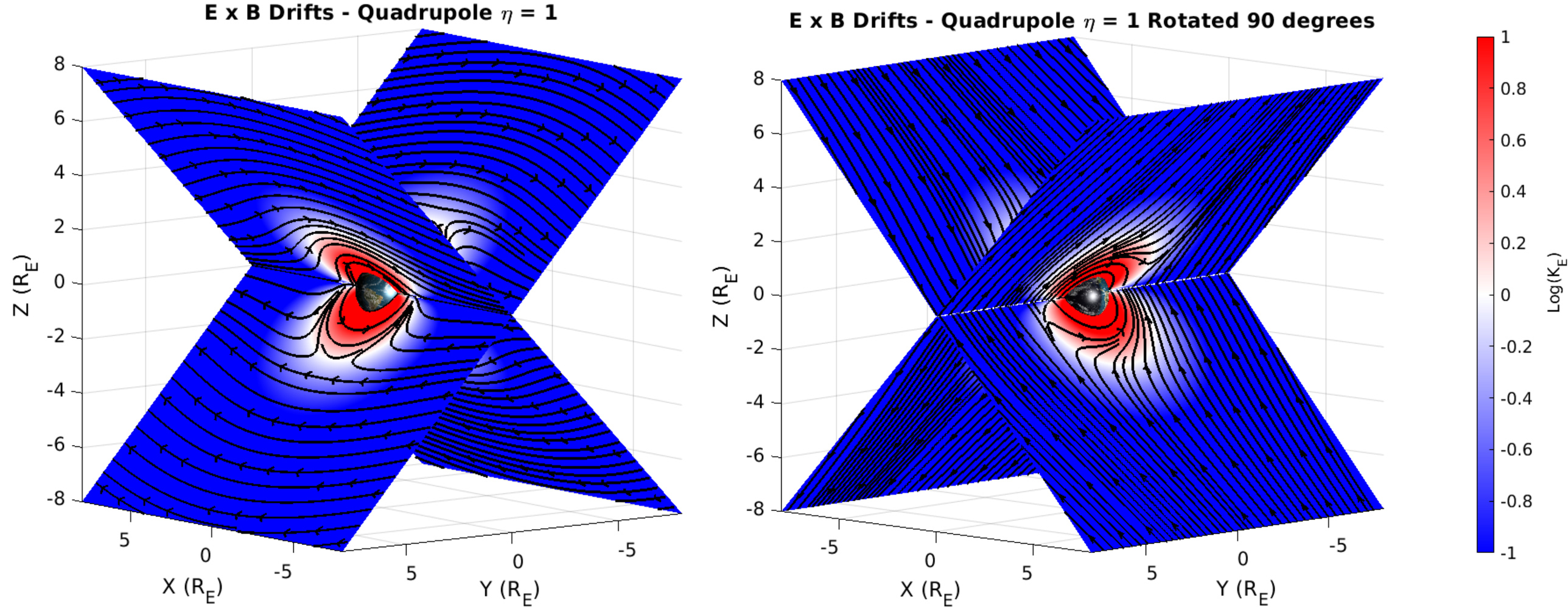
E x B Drifts - Quadrupole η = 1
E x B Drifts - Quadrupole η = 1 Rotated 90 degrees
Z (R_E)
X (R_E)
Y (R_E)
Log(K_E)
8
6
4
2
0
-2
-4
-6
-8
5
0
-5
1
0.8
0.6
0.4
0.2
0
-0.2
-0.4
-0.6
-0.8
-1

Figure 6.

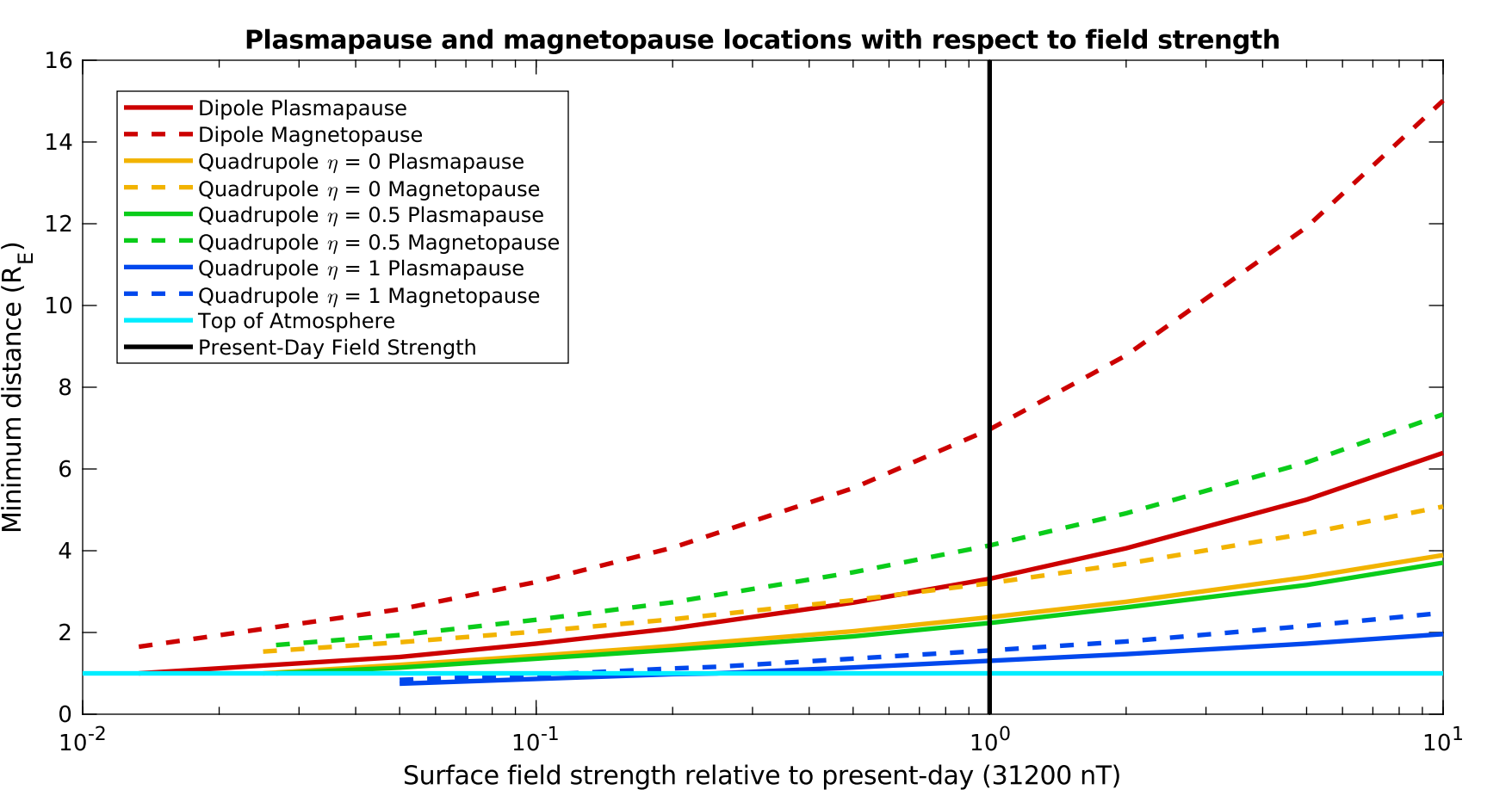
Plasmapause and magnetopause locations with respect to field strength
Dipole Plasmapause
Dipole Magnetopause
Quadrupole η = 0 Plasmapause
Quadrupole η = 0 Magnetopause
Quadrupole η = 0.5 Plasmapause
Quadrupole η = 0.5 Magnetopause
Quadrupole η = 1 Plasmapause
Quadrupole η = 1 Magnetopause
Top of Atmosphere
Present-Day Field Strength
Minimum distance (R_E)
Surface field strength relative to present-day (31200 nT)
0
2
4
6
8
10
12
14
16
10^-2
10^-1
10^0
10^1

Figure A.

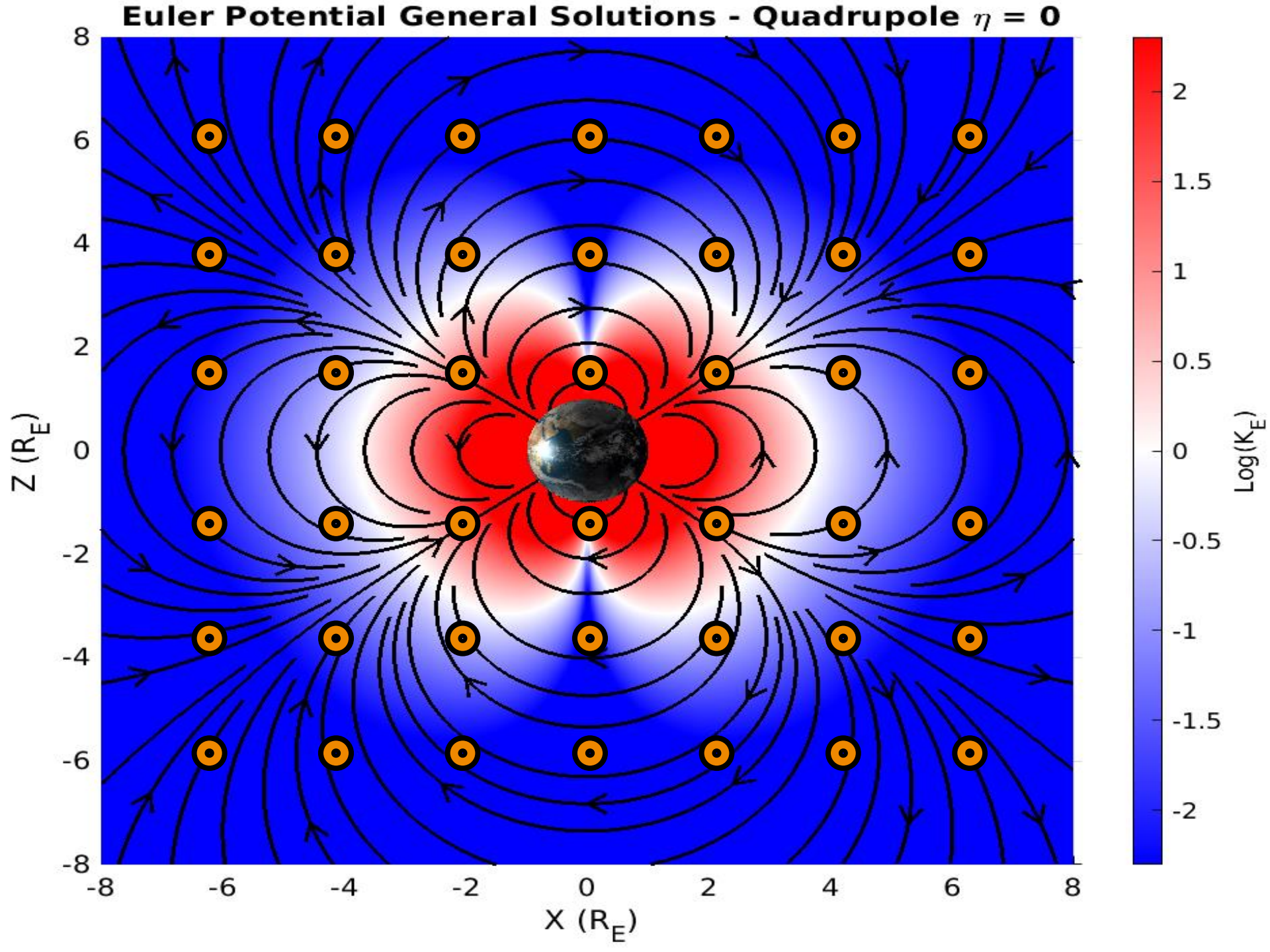
Euler Potential General Solutions - Quadrupole $\eta = 0$
8
6
4
2
0
-2
-4
-6
-8
Z (R_E)
-8
-6
-4
-2
0
2
4
6
8
X (R_E)
2
1.5
1
0.5
0
-0.5
-1
-1.5
-2
Log(K_E)